

GENERAL RELATIVISTIC RADIATION MAGNETOHYDRODYNAMICS SIMULATIONS OF
SUPERCritical ACCRETION ONTO MAGNETIZED NEUTRON STAR; -MODELLING OF ULTRA
LUMINOUS X-RAY PULSARS

HIROYUKI R. TAKAHASHI¹ AND KEN OHSUGA^{2,3}

¹*Center for Computational Astrophysics, National Astronomical Observatory of Japan, National Institutes of Natural Sciences, Mitaka, Tokyo 181-8588, Japan*

²*Division of Theoretical Astronomy, National Astronomical Observatory of Japan, National Institutes of Natural Sciences, Mitaka, Tokyo 181-8588, Japan*

³*School of Physical Sciences, Graduate University of Advanced Study (SOKENDAI), Shonan Village, Hayama, Kanagawa 240-0193, Japan*

(Received July 1, 2016; Revised September 27, 2016; Accepted July 27, 2017)

ABSTRACT

By performing 2.5-dimensional general relativistic radiation magnetohydrodynamic simulations, we demonstrate supercritical accretion onto a non-rotating, magnetized neutron star, where the magnetic field strength of dipole fields is 10^{10} G on the star surface. We found the supercritical accretion flow consists of two parts; the accretion columns and the truncated accretion disk. The supercritical accretion disk, which appears far from the neutron star, is truncated at around $\simeq 3R_*$ ($R_* = 10^6$ cm is the neutron star radius), where the magnetic pressure via the dipole magnetic fields balances with the radiation pressure of the disks. The angular momentum of the disk around the truncation radius is effectively transported inward through magnetic torque by dipole fields, inducing the spin up of a neutron star. The evaluated spin up rate, $\sim -10^{-11}$ s s⁻¹, is consistent with the recent observations of the ultra luminous X-ray pulsars. Within the truncation radius, the gas falls onto neutron star along dipole fields, which results in a formation of accretion columns onto north and south hemispheres. The net accretion rate and the luminosity of the column are $\simeq 66L_{\text{Edd}}/c^2$ and $\lesssim 10L_{\text{Edd}}$, where L_{Edd} is the Eddington luminosity and c is the light speed. Our simulations support a hypothesis whereby the ultra luminous X-ray pulsars are powered by the supercritical accretion onto the magnetized neutron stars.

Keywords: accretion, accretion disks — stars: neutron — magnetohydrodynamics — methods: numerical

arXiv:1707.07356v2 [astro-ph.HE] 26 Jul 2017

1. INTRODUCTION

Accretion disks around compact objects such as neutron stars or black holes are one of the most energetic system in the universe. The disk is powered by liberating the gravitational energy, so that the mass accretion rate is an important key parameter determining their activities. Theoretically, there are three distinct accretion modes according to mass accretion rate, e.g., the radiatively inefficient accretion flow (Narayan & Yi 1994), standard disk (Shakura & Sunyaev 1976), and slim disk (Abramowicz et al. 1988). The mass accretion rate of the slim disk, which is the highest among three modes, is higher than the critical rate ($\dot{M}_{\text{crit}} = L_{\text{Edd}}/c^2$) where L_{Edd} is the Eddington luminosity and c is the light speed. The luminosity of the slim disk exceeds the Eddington luminosity, so that the slim disk is applied to the very luminous objects. One of the possible site of the supercritical accretion is the Ultra luminous X-ray sources (ULXs). It is well known that ULXs show super-Eddington luminosity for the stellar mass black hole. Thus, it has been suggested that the supercritical accretion occurs in the ULXs. But the another solution with sub-critical accretion onto an intermediate mass black hole is possible. It is still under debate which is feasible to explain characteristics of ULXs.

A recent finding of pulsation in ULXs changes the situation. Bachetti et al. (2014) found a X-ray pulsation with period of $P = 1.37$ s and its time derivative $\dot{P} = -2 \times 10^{-10}$ s s $^{-1}$ from M82 X-2. After this notable discovery, X-ray pulsations have been observed in other two ULXs, of which the spin up rate is reported to be $\sim -4 \times 10^{-11}$ s s $^{-1}$ and $\sim -5 \times 10^{-9}$ s s $^{-1}$ (Israel et al. 2016; Fürst et al. 2016; Israel et al. 2017). These observational facts indicate that a supercritical accretion onto a pulsar (namely, ULX Pulsars), since the luminosity of these ULXs highly exceeds the Eddington luminosity for the neutron stars.

Ohsuga (2007) performed radiation hydrodynamics simulations of supercritical disk accretion onto a non-magnetized neutron star. After that Takahashi & Ohsuga (2017) performed general relativistic radiation magnetohydrodynamics (GR-RMHD) simulations of the supercritical disks around a non-magnetized neutron star. They showed a formation of powerful outflows from the vicinity of the neutron star. Since the neutron star, different to the black hole, does not swallow the mass and energy, the resulting outflow power is stronger than the black hole (see, also King & Lasota 2016). However, in these study, the neutron star magnetic field is ignored, although observations of the $P - \dot{P}$ relations reveal the existence of the strong field (Bachetti et al. 2014).

If the neutron star magnetic field is strong enough to prevent the disk accretion, the matter would fall onto the neutron star along the magnetic field lines. Basko & Sunyaev (1976) proposed a model of the supercritical column accretion onto the neutron star. Also, Kawashima et al. (2016) performed radiation hydrodynamic simulation of supercritical accretion column. The interaction between neutron star magnetic fields and accretion disks is, however, unresolved in such local simulations. Thus, the global radiation magnetohydrodynamic simulation is necessary to reveal the global structure of the supercritical accretion flows around the neutron star by taking into consideration the interaction between radiation dominated accretion disks and neutron star magnetosphere. Then, the general relativistic effects also should be taken into account, since the neutron star radius is comparable to its gravitational radius, and since Alfvén speed in the magnetosphere would be close to the light speed via the strong magnetic field. Fortunately, GR-RMHD code has been developed by authors (McKinney et al. 2014; Sądowski et al. 2014; Sądowski & Narayan 2015; Takahashi et al. 2016; Sądowski et al. 2017). The previous work, including this study, assume the equation of state for radiation field to close the system (Levermore 1984). The M-1 closure is useful to include effects of radiation such as energy and momentum exchange between the gas and radiation, but there are some limitations in this approximation. The discussion on this limitation is shown in section 4.

In this paper, we adopted the moment formalism on radiation field for the first step and we report our results of 2.5-dimensional global GR-RMHD simulations of the supercritical accretion flows around the neutron stars with strong dipole magnetic field. Our results show that the supercritical accretion onto the magnetized neutron star is plausible model for the ULX pulsars.

2. METHODS

We solved GR-RMHD equations by adopting moment formalism describing radiation field (Thorne 1981). Basic equations and numerical schemes are the same with our former papers (Takahashi et al. 2016). We incorporate the mean electron scattering, free-free emission, thermal Comptonization (Sądowski et al. 2015), and synchrotron emission (Sądowski et al. 2017) for the source of opacity.

We solved GR-RMHD equations in polar coordinate (t, r, θ, ϕ) with Boyer-Lindquist metric by assuming axisymmetry with respect to a rotation axis $\theta = 0, \pi$. The computational box consists of $r = [R_*, 199R_*]$ and $\theta = [0, \pi]$, where

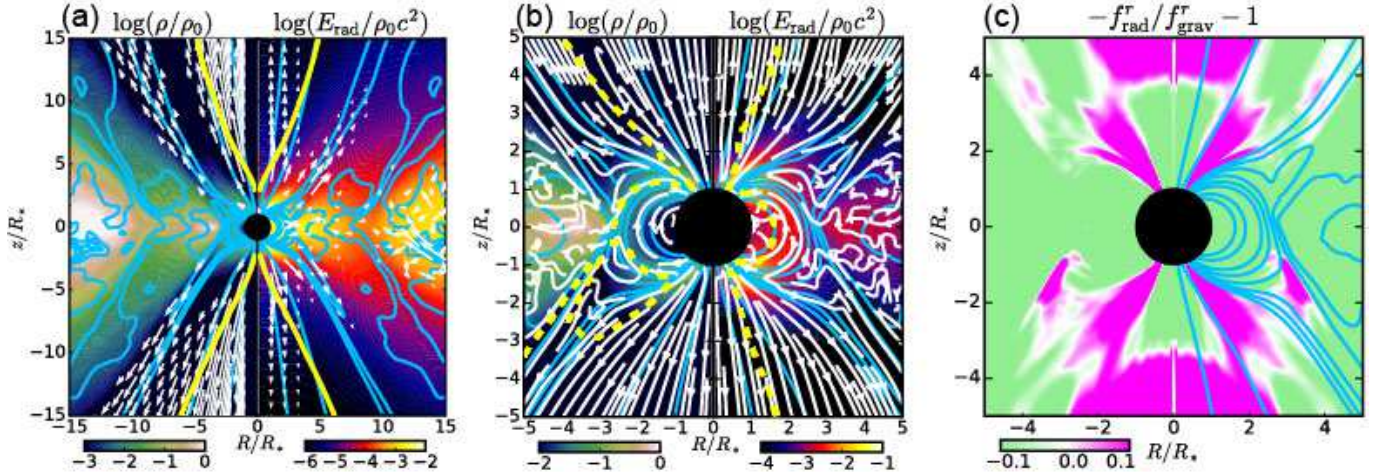


Figure 1. a: Colors show ρ/ρ_0 (left) and $E_{\text{rad}}/\rho_0 c^2$ (right), while vectors show the four velocity (left) and radiation flux (right). Blue lines are magnetic field lines and yellow lines show the photosphere measured from poles. b: enlarged view of figure 1a, but white curves show stream lines of four velocity (left) and radiation flux (right). The yellow dashed curves show $\beta = 1$ (left) and $\sigma = 1$ (right). c: Color shows $-f_{\text{rad}}^r/f_{\text{grav}}^r - 1$.

$R_* = 10$ km is a neutron star radius. The radial grid exponentially increases with radius and the uniform grid is adopted in θ -direction. Numerical grid points are $(N_r, N_\theta, N_\phi) = (528, 288, 1)$.

The neutron star mass is assumed to be $M_* = 1.4M_\odot$. We adopt a dipole magnetic field (Wasserman & Shapiro 1983), of which strength is fixed to be $B_* = 10^{10}$ G at the neutron star surface. The magnetic axis is assumed to coincide with the rotation axis. We suppose the non-rotating neutron star in the present study for simplicity. This assumption would be valid since the observed rotation velocity of the neutron star is slower than the Keplerian velocity. The study for the case of the rapidly rotating neutron star is left as important future work.

We set an equilibrium torus given by Fishbone & Moncrief (1976), but the gas pressure is replaced by the sum of gas (p_{gas}) and radiation (p_{rad}) pressure assuming local thermodynamic equilibrium. The inner edge and pressure maximum of the torus are located at $r = 10R_*$ and $r = 15R_*$, respectively. We employ the maximum density of the torus ρ_0 of 0.1 g cm^{-3} . In addition to the dipole magnetic field of the neutron star, the poloidal magnetic field confined in this torus is embedded so that its magnetic flux vector A_ϕ is proportional to the density. The confined magnetic fields are anti-parallel to dipole fields at the inner part of the torus (but, see Romanova et al. 2011, for the difference of parallel and anti-parallel cases). The ratio of maximum $p_{\text{gas}} + p_{\text{rad}}$ to the maximum magnetic pressure (p_{mag}) via the confined magnetic fields is set to be 100. We also give a perturbation on $p_{\text{gas}} + p_{\text{rad}}$ by its 10% to break an equilibrium state.

The neutron star and the torus are initially surrounded by a relatively low density corona. Its density decreases with radius as $\rho = \rho_c (R_*/r)^3$, where ρ_c is set as an initial coronal σ parameter becomes $\sigma_c = B_*^2/(4\pi\rho_c c^2) = 500$. The gas pressure of the corona is $p_{\text{gas}} = 0.1\rho c^2$.

We adopted a symmetric boundary condition at $\theta = 0, \pi$, and outflow boundary condition at $r = 199R_*$. For the inner boundary ($r = R_*$), the velocity and radiation flux are set to be zero. A free boundary condition is applied to the other quantities (Romanova et al. 2011). The outgoing boundary condition is applied at outer boundary.

3. RESULTS

After simulation starts, an initial equilibrium state gradually breaks due to a given perturbation. The accreting matter reaches a neutron star surface at $t = 4,800t_g$, where $t_g = GM_*/c^3 = 6.9 \times 10^{-6}$ s is the light crossing time of the gravitational radius. After that, the mass accretion rate is almost kept constant until simulation stops at $t = 15,000t_g$. Figure 1a shows global structure of inflow and outflow around magnetized neutron star on $(R, z) = (r \sin \theta, r \cos \theta)$ plane. Color shows ρ/ρ_0 (left) and $E_{\text{rad}}/\rho_0 c^2$ (right), while arrows show four velocity of fluid (left) and radiation flux (right). Blue lines indicate magnetic field lines. In figures 1, 2, and table 1, all the data are averaged in time between $[10^4 t_g, 1.5 \times 10^4 t_g]$. We find an accretion disk is formed at the region of $3R_* \lesssim r \lesssim 8R_*$ (white region

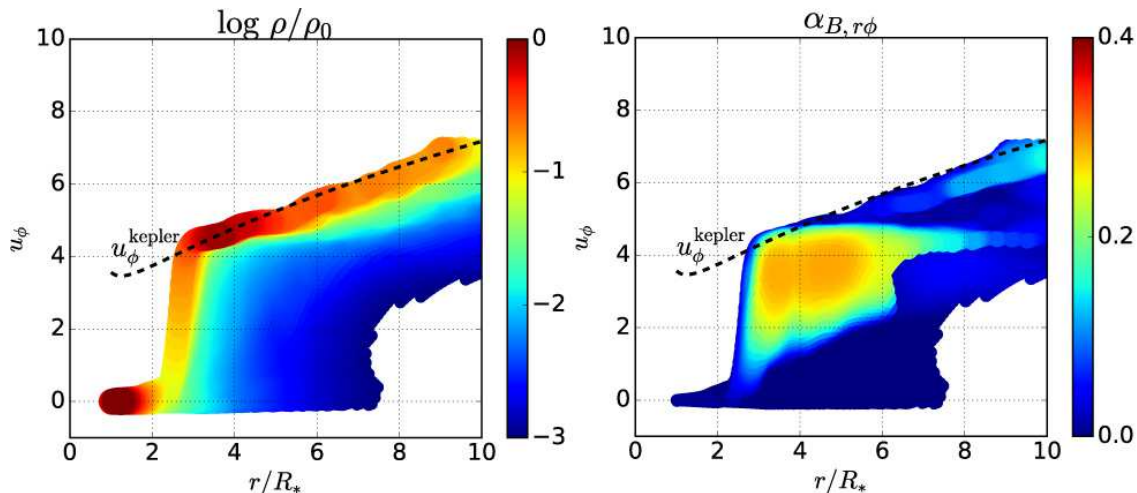


Figure 2. Density (left) and $\alpha_{B,r\phi}$ (right) plots on $r - u_\phi$ plane. Black dashed line shows Keplerian velocity.

near the equatorial plane). The disk density on the equatorial plane is about $0.1\rho_0 = 0.01 \text{ g cm}^{-3}$. The radiation energy is enhanced in the disk (see yellow region in the right panel) and dominates the other energy. Inside the disk, magnetic fields are tangled due to the development of magnetorotational instability (MRI) (Hawley & Balbus 1991; Balbus & Hawley 1991, 1998). The induced turbulent motion is clearly shown in the left panel in figure 1b (stream lines of four velocity shown with white curves). Here we note that the high density region at $r \gtrsim 8R_*$ is the remnant of the initial torus.

White arrows in the left panel means that strong jets are ejected around the rotation axis. The jets have an opening angle of $\lesssim 18^\circ$ and typical speed is $0.4c$ at $|z| \sim 30R_*$. These fast jets are ejected due to the radiation force (Takahashi & Ohsuga 2015). Indeed, we find that the outward radiation flux is enhanced around the rotation axis. Besides fast jets, relatively slow and dense outflows are ejected in the direction of $\theta = 40^\circ$ and 140° , even though the boundary between the jet and the outflow is not clear since the density as well as the velocity smoothly change in theta-directions. Such outflows have velocity of $\simeq 0.1c$ around $r = 30R_*$, and its density is about two orders of magnitude higher than fast jets. The outflows are also driven by the radiation force. We find the slightly enhanced radiation flux in the outflow region (see right panel). In outflow region, the recurrent magnetic reconnections occur (Ferreira et al. 2006; Romanova et al. 2011) even though we applied ideal MHD. The reconnections also help the outflow acceleration (Hayashi et al. 1996; Kato et al. 2004).

For a smaller radius, an interaction of dipole magnetic field and disk is manifest. Figure 1b is an enlarged view of figure 1a. We plot by yellow dashed lines $\beta = (p_{\text{gas}} + p_{\text{rad}})/p_{\text{mag}} = 1$ (left panel) and $\sigma \equiv b^2/(4\pi\rho c^2) = 1$, where $b^2 = 8\pi p_{\text{mag}}$ (right panel). The magnetic energy dominates the other energy around the rotation axis. In addition, we find the region of $\beta < 1$ near the neutron star for $25^\circ \lesssim \theta \lesssim 155^\circ$ (magnetosphere). The right panel in figure 1b clearly shows that σ value is very large near the neutron star as well as around the rotation axis. Typically, we find $\sigma \sim 100$ deep inside the magnetosphere and $\sigma \sim 150$ around poles. Since the ideal MHD is assumed in the present simulations, the disk matter cannot enter the magnetosphere. Hence, the accretion disk is truncated around $r_T \simeq 3R_*$. At the truncation radius, the magnetic reconnection takes place between the dipole field and disk field. As noted before, we assume that the magnetic polarity between these fields is anti-parallel. The magnetic reconnection at the truncation radius leads to the mass transfer from disks to the magnetosphere (Romanova et al. 2011). Inside the truncation radius, the matter accretes along the magnetic field lines, producing the accretion columns in north and south hemispheres around $\theta = 25^\circ$ and 155° (Ghosh & Lamb 1979) (see green region near the neutron star surface in the left panel). The flow is turbulent in the accretion disk, while it is relatively laminar in accretion columns (see left panel in figure 1b). In classical theories applied for T-tauri stars, white dwarfs and neutron stars, the magnetospheric radius is determined by a balance between the magnetic pressure of dipole fields and the gas (plus ram) pressure. For the supercritical flows, the radiation pressure dominates the other energy. Thus the magnetospheric radius of accretion disks is determined by the magnetic pressure and the radiation pressure.

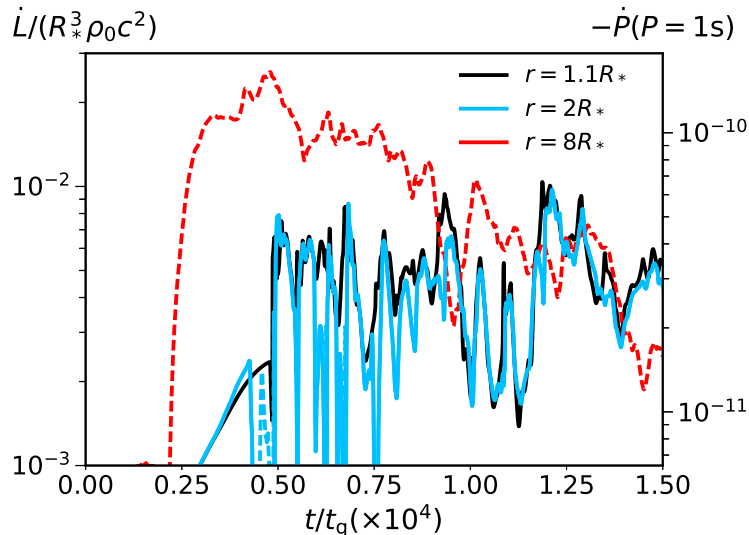


Figure 3. time evolution of angular momentum flux at $r = 1.1R_*$ (black), $r = 2R_*$ (blue), $r = 3R_*$ (orange) and $r = 8R_*$ (red). Solid lines show negative flux and dashed ones do positive flux.

Lyutikov (2014) showed that the radiation force prohibits from mass accretion for relatively low mass accretion rate case. In contrast, the radiation force does not prevent the mass accretion in the accretion columns and the accretion rate largely exceeds the critical rate in our model. Figure 1-c shows a ratio of radial component of radiation force and gravity force. The outward radiation force is smaller than the gravity inside the accretion columns (see green region between $40^\circ \lesssim \theta \lesssim 140^\circ$). In contrast, we found the radiation force overcomes the gravity force just above (below) the accretion column in northern (southern) hemisphere (see magenta region between $10^\circ \lesssim \theta \lesssim 40^\circ$ and $140^\circ \lesssim \theta \lesssim 170^\circ$). This is thought to be caused by that the radiation energy escapes from side walls of accretion columns, which reduces (enhances) the radiation energy inside (outside) the accretion columns. Thus, the mass accretion is feasible inside the column, in contrast, the gas is blown away by the strong radiation force outside the column. In addition, the large optical thickness of the column helps the matter accretes. The optical depth inside accretion columns largely exceeds unity, so that the radiation energy is transported by the radiative diffusion. Then, radiation flux and the radiation flux force tend to be suppressed. Such situation is basically same as that in Kawashima et al. (2016) in which the super-Eddington accretion column of which the optical depth is much larger than unity was realized by the escape of the radiation energy from the side wall of the column. Ohsuga & Mineshige (2007) also reported that the super-Eddington disk accretion is feasible via the anisotropy and the large optical thickness.

In table 1, we show mass accretion rate, outflow rate, net inflow rate (accretion rate - outflow rate), and bolometric luminosity measured at $r = 1.1R_*$, $3R_*$ and $8R_*$. The mass accretion rate as well as the net inflow rate exceeds the critical rate. This means that the supercritical accretion occurs not only the disk ($\gtrsim 3R_*$) but also accretion columns ($\lesssim 3R_*$). Although the net inflow rate is around $10\dot{M}_{\text{crit}}$ at $r = 1.1R_*$, $3R_*$, it is $\sim 300\dot{M}_{\text{crit}}$ at $r = 8R_*$. This implies that the large amount of the accreting matter accumulates in the disk region, $3R_* \lesssim r \lesssim 8R_*$, and a part of the matter accretes onto the neutron star through the accretion columns. When the density around the truncation radius drastically increases via the accumulation of the matter, the flow structure might change. For instance, the high density matter flows into the columns and the mass accretion rate onto the star surface might greatly increase. Or, the magnetosphere might be crushed by the strengthened gas and radiation pressure. We need long-term simulations in order to make clear the point.

The resulting bolometric luminosity largely exceeds the Eddington luminosity as shown in the table 1. Since L_{bol} at $r = 3R_*$ is comparable to or slightly larger than that at $r = 8R_*$, it is thought that the radiation is mainly generated near the neutron star. The right panel in figure 1b shows that the radiation energy is drastically enhanced in the accretion columns, and a strong outward radiation flux appears outside the columns. The formation of very luminous accretion columns has also been proposed by authors (Basko & Sunyaev 1976; Kawashima et al. 2016). At the outer

region of $r \gtrsim 10R_*$, the outward radiation flux is enhanced around the rotation axis (see the right panel of figure 1a). Thus, this object would be identified as highly super-Eddington source for the face-on observer.

Left panel of figure 2 shows distribution of a gas density in $r - u_\phi$ plane. Here u_ϕ is the ϕ -component of covariant four velocity. In this figure, only a high density ($\rho > 10^{-3}\rho_0$) region is plotted. For $r > r_T$, a dense gas inside accretion disks (red and orange) is located around the dotted line. This means that the rotation velocity of the disk matter is close to the Keplerian velocity. Around the truncation radius, the angular momentum suddenly decreases and it goes to zero on the neutron star surface. That is, the matter in the accretion columns rotates slowly. This is because that the angular momentum of the accreting matter is quickly transported to the neutron star via the magnetic torque of dipole fields. This is understood from the right panel of figure 2, in which we show a viscous parameter evaluated by $\alpha_{B,r\phi} = T_{\text{mag}}^{\tilde{r}\tilde{\phi}} / (p_{\text{gas}} + p_{\text{rad}} + p_{\text{mag}})$. Here, $T_{\text{mag}}^{\tilde{r}\tilde{\phi}}$ is a $r - \phi$ component of energy momentum tensor of electromagnetic field (Penna et al. 2010), and the tilde indicates a comoving frame quantity. This panel shows $\alpha_{B,r\phi}$ is about or less than 0.1 in the disk region (near the dotted line for $r \gtrsim 5R_*$). Such a small viscosity is consistent with GR-MHD simulations (Penna et al. 2013). We also find a relatively large $\alpha_{B,r\phi}$ region (orange) near the truncation radius. As shown in figure 2b, the strong magnetic field lines in this region connect to the neutron star surface. Since the non-rotating neutron star is employed in the present work, the magnetic torque of dipole fields effectively extract the angular momentum of the matter.

We plot the angular momentum flux computed by

$$\dot{L} = \int T_{\text{mag}\phi}^r \sqrt{-g} d\theta d\phi, \quad (1)$$

(Romanova et al. 2009), where g is the determinant of the metric. Black, blue, and red lines corresponds to the angular momentum flux measured normalized by $R_*^3 \rho_0 c^2$ at $r = 1.1R_*$, $2R_*$, and $8R_*$. Solid lines show inward flux and dashed lines indicate outward flux. Here we only consider an angular momentum flux contributed from magnetic fields since the kinetic and radiation terms are negligible even in the radiation dominated disk. Far from the truncation radius ($r = 8R_*$), the angular momentum is transported outward due to the MRI turbulence. Inside $r \simeq r_T$ ($r = 1.1R_*$ and $2R_*$), the angular momentum flux is negative throughout simulations. Thus the angular momentum of the disk is extracted through the dipole field, leading to spin up of a neutron star. If we assume the rotation period of neutron star to be 1 s, the spin up period estimated from our result $\dot{L} = 0.04R_*^3 \rho_0 c^2$ corresponds to $\dot{P} \sim -3 \times 10^{-11} \text{ s s}^{-1}$. This result is consistent with the observations of ULX pulsars, from $\sim -5 \times 10^{-9} \text{ s s}^{-1}$ to $\sim -4 \times 10^{-11} \text{ s s}^{-1}$.

4. CONCLUSION & DISCUSSION

In this paper, we first demonstrate a supercritical accretion onto a non-rotating magnetized neutron star using 2.5-dimensional GR-RMHD simulations. We show that radiation dominated accretion disks are formed far from a neutron star, and are truncated around $r = r_T = 3R_*$. Inside this radius, the accretion columns form and the matter accretes onto north and south hemisphere of the neutron star. The truncation radius of the radiation dominated disk is determined by the radiation pressure and the magnetic pressure via the dipole fields of the neutron star. Indeed, we find that the radiation pressure is comparable to the magnetic pressure at $r \sim r_T$. Also we found fast jets ($\sim 0.4c$) along the rotation axis ($\lesssim 20^\circ$ and $\gtrsim 160^\circ$). Besides fast jets, relatively slow ($\sim 0.1c$) and dense outflows are emanated with larger opening angle, $\sim 40^\circ$. Both jets and outflows are accelerated by the radiation force.

We show that a resulting luminosity exceeds the Eddington luminosity, $\sim 10L_{\text{Edd}}$. This radiation flux is marginally collimated around the disk and magnetic rotation axis, $\theta = 0$ and π . The e -folding angle of the luminosity, which corresponds to the beaming factor b , is about 0.2 at $150R_*$. This beaming factor is larger than that proposed by (King & Lasota 2016). They showed that the beaming factor decreases with mass accretion rate $b \propto \dot{M}^{-2}$ (Rykoﬀ et al. 2009). We do not know the reason of this discrepancy, but one possibility is that the massive outflows with a large opening angle decreases the beaming factor due to the electron scattering. The dependence of the mass accretion rate on the luminosity, beaming factor and accretion mode will be reported in the subsequent paper.

As we have mentioned above, the spin up rate obtained by our simulations, $\dot{P} \sim -10^{-11} \text{ s s}^{-1}$, is consistent with the observations. Such a suitable spin up rate is naturally understood by the interaction of the neutron star magnetic fields and supercritical accretion disks. The spin up rate is estimated by $\dot{P} = -\dot{M}l(r_m)/M_*l_*$, (Shapiro & Teukolsky 1986), where l and l_* are angular momentum of disk matter and neutron star, and r_m is the magnetospheric radius. The magnetospheric radius is obtained by the balance between the magnetic pressure of dipole fields and the radiation pressure of the disk for the case of the radiation dominated accretion disks. Applying self-similar solutions for slim disk (Watarai & Fukue 1999), the magnetospheric radius is obtained as $r_m/R_* \simeq$

$1.7(\alpha/0.1)^{2/7}(\dot{M}/10^2\dot{M}_{\text{crit}})^{-2/7}(B_*/10^{10}\text{G})^{4/7}(M_*/1.4M_\odot)^{-3/7}(R_*/10\text{km})^{5/7}$, where α is the viscous parameter. Note that the magnetospheric radius is smaller than the corotation radius, $r_{\text{cor}}/R_* = 170(M_*/1.4M_\odot)^{1/3}(P_*/1\text{ s})^{2/3}$ where P_* is the rotation period of the neutron star. The magnetospheric radius is a decreasing function of \dot{M} . The magnetosphere would disappear for a sufficiently high mass accretion rate and the accretion disks reach to a neutron star surface (Ohsuga 2007). The spin up rate is estimated by assuming that the Keplerian angular momentum at the magnetospheric radius is transported to neutron star without dissipation, as $\dot{P} \simeq -4.9 \times 10^{-11}(\alpha/0.1)^{1/7}(\dot{M}/10^2\dot{M}_{\text{crit}})^{6/7}(B_*/10^{10}\text{G})^{2/7}(M_*/1.4M_\odot)^{2/7}(R_*/10\text{km})^{-8/7}(P_*/1\text{s})\text{ss}^{-1}$. This is comparatively near to the spin up rate obtained by the present simulations, and is consistent with observations of ULX pulsars. Hence, we stress again that our present simulations reveal that the ULX pulsars can be explained by the supercritical accretion onto the magnetized neutron stars.

The net inflow rate in the accretion columns is about ten times larger than the critical rate, and the resulting bolometric luminosity is several $\times L_{\text{Edd}}$. Since the outward radiative flux is sensitive to the polar angle, the observed luminosity notably depends on the observer's viewing angle. The supercritical accretion flow around the magnetized neutron star tends to be identified as highly super-Eddington source since the radiative flux is enhanced around the magnetic axis. In this study, we assume that the magnetic axis is parallel to the rotation axis of the disks. Also, the non-rotating neutron star is supposed. Thus, observed luminosity does not exhibit a periodic modulation of the luminosity, which implies that our present model cannot explain ULX pulsars. However, if the magnetic dipole axis is misaligned with neutron star rotation axis and the neutron star rotates, the observed luminosity varies with the rotation period of the neutron star. If this is the case, our results would support the hypothesis whereby the ULX pulsars are powered by the supercritical accretion onto the magnetized neutron stars. Such argument would be confirmed by three-dimensional simulations.

We show that the net mass accretion rate is not constant, but it increases for a larger radius ($r > 8R_*$). The non-steady accretion, especially non-uniform net mass accretion rate at larger radius, is caused by the shortage of computational time. We initially set equilibrium torus at $r > 10R_*$. This gas torus gradually falls onto the neutron star due to the development of MRI. Since the dynamical timescale is longer for larger radius, the system tends to become steady from the smaller radius. Thus, the equilibrium radius, where the net mass inflow rate is constant, would extend by long term simulations, although a steady state is not realized for a larger radius $\gtrsim 8R_*$ in the present simulations. However, such long term simulations are time-consuming and study of long term evolution of disks is beyond of scope of this paper.

If such long term simulations are realized, the accretion rate might increase due to the accretion of the remnant of the initial torus. Then, the magnetosphere would shrink gradually. When the mass accretion rate is sufficiently high, the radiation pressure of the disks overcomes the magnetic pressure. Then the magnetosphere disappears and supercritical disk accretion would be realized (Ohsuga 2007).

It is noted that an effect of boundary condition would affect on results for a long term simulations. We observed a gradual increase in mass density on the neutron star surface. This is caused by the reflection boundary condition by which the matter tends to accumulate around the neutron star surface. Therefore, the mass density near the surface would be larger in the long term simulations. If we adopt free boundary condition, the mass is swallowed by the inner boundary and the increase of the mass density would not occur. Such a boundary condition is adopted by authors (e.g. Romanova et al. 2012).

We adopted a truncation formalism for radiation field by adopting the M-1 closure. The M-1 closure is useful to describe the radiation field in optically thick limit and optically thin free-streaming limit. Also since the computational cost is reasonably small, the M-1 closure is adopted in many astrophysical fields. However, we caution that adopting M-1 closure is sometimes not validated especially in optically thin, anisotropic case. Since the moment formalism is obtained by integrating transfer equation in solid angles, two radiation beams unphysically collides each other (e.g., for example Ohsuga & Takahashi 2016). A similar situation might happen in our simulations, since the two accretion columns (north and south) are main light sources. The photons emitted by the north accretion columns can collide with that emitted by the south accretion column around an equatorial plane. The photons propagate in radial direction after collision. The radial stream lines of radiation flux between two accretion columns might be caused by such collision (see $r < 1.5R_*$ in the lower latitude in the right panel of figure 1-b). Such unphysical collision might affect on accretion dynamics. If the photon collision does not occur, two accretion columns illuminate each other. The radiation force might induce the time variability and/or oscillation of accretion columns. However, it is difficult to conclude whether radial profiles of stream line is a consequence of unphysical merging of radiation flux. Even if the

	$\dot{M}_{\text{in}}/M_{\text{crit}}$	$\dot{M}_{\text{out}}/M_{\text{crit}}$	$\dot{M}_{\text{out}}/M_{\text{in}}$	$L_{\text{bol}}/L_{\text{Edd}}$
$r = 1.1R_*$	66	55	0.84	6.1
$r = 3R_*$	301	291	0.97	9.0
$r = 8R_*$	1350	935	0.69	7.0

NOTE— From left to right, mass accretion rate, outflow rate, its ratio, and bolometric luminosity. Values measured at $r = 1.1, 3, 8R_*$, are time averaged between $t = 10^4 t_g$ and $t = 1.5 \times 10^4 t_g$.

photons pass through without collision, the θ -component of the radiation flux becomes very small. Then, stream lines of radiation flux would be almost radial, although two photons never merge.

Also the M-1 closure cannot treat radiative viscosity correctly. Numerical studies showed that an efficiency of angular momentum transport by MRI-driven turbulence depends on the magnetic Prandtl number (Lesur & Longaretti 2007; Fromang et al. 2007; Simon & Hawley 2009) Jiang et al. (2013) performed MHD simulations with frequency integrated radiation transfer equation and show that radiative viscosity significantly exceeds microscopic viscosity and magnetic resistivity in the context of local shearing box approximation. But they also showed that it is still negligible compared to Maxwell stress and Reynolds stress. On the other hand, we show that the angular momentum of the gas inside accretion column is transported to the neutron star and is small due to the magnetic torque by the dipole field. Thus the radiative viscosity might not affect on the accretion dynamics both in accretion column and accretion disks. Even though that, we have to solve transfer equation for radiation to resolve these problems. Jiang et al. (2014) performed radiation magnetohydrodynamics simulations by solving frequency-integrated transfer equations. They observed a lower radiative efficiency than that of GR-RMHD results. But we need to pay attention that they assume non-relativistic plasma. The discrepancy requires further investigation. Ohsuga & Takahashi (2016) developed a numerical method solving transfer equation in the framework of the special relativity. Solving the transfer equation including the general relativistic effect has not been succeeded yet and is the grand challenge to understand accretion disks onto the black hole and neutron star. We will tackle on this problem in a near future.

Numerical computations were carried out on Cray XC30 at the Center for Computational Astrophysics of National Astronomical Observatory of Japan, on FX10 at Information Technology Center of the University of Tokyo, and on K computer at AICS. This work is supported in part by JSPS Grant-in-Aid for Young Scientists (17K14260 H.R.T.) and for Scientific Research (C) (15K05036 K.O.). This research was also supported by MEXT as 'Priority Issue on Post-K computer' (Elucidation of the Fundamental Laws and Evolution of the Universe) and JICFuS.

REFERENCES

- Abramowicz, M. A., Czerny, B., Lasota, J. P., & Szuszkiewicz, E. 1988, *ApJ*, 332, 646
- Bachetti, M., Harrison, F. A., Walton, D. J., Grefenstette, B. W., Chakrabarty, D., Fürst, F., Barret, D., Beloborodov, A., Boggs, S. E., Christensen, F. E., Craig, W. W., Fabian, A. C., Hailey, C. J., Hornschemeier, A., Kaspi, V., Kulkarni, S. R., Maccarone, T., Miller, J. M., Rana, V., Stern, D., Tendulkar, S. P., Tomsick, J., Webb, N. A., & Zhang, W. W. 2014, *Nature*, 514, 202
- Balbus, S. A. & Hawley, J. F. 1991, *ApJ*, 376, 214
- . 1998, *Reviews of Modern Physics*, 70, 1
- Basko, M. M. & Sunyaev, R. A. 1976, *MNRAS*, 175, 395
- Ferreira, J., Dougados, C., & Cabrit, S. 2006, *A&A*, 453, 785
- Fishbone, L. G. & Moncrief, V. 1976, *ApJ*, 207, 962
- Fromang, S., Papaloizou, J., Lesur, G., & Heinemann, T. 2007, *A&A*, 476, 1123
- Fürst, F., Walton, D. J., Harrison, F. A., Stern, D., Barret, D., Brightman, M., Fabian, A. C., Grefenstette, B., Madsen, K. K., Middleton, M. J., Miller, J. M., Pottschmidt, K., Ptak, A., Rana, V., & Webb, N. 2016, *ApJL*, 831, L14
- Ghosh, P. & Lamb, F. K. 1979, *ApJ*, 234, 296
- Hawley, J. F. & Balbus, S. A. 1991, *ApJ*, 376, 223

- Hayashi, M. R., Shibata, K., & Matsumoto, R. 1996, *ApJL*, 468, L37+
- Israel, G. L., Belfiore, A., Stella, L., Esposito, P., Casella, P., De Luca, A., Marelli, M., Papitto, A., Perri, M., Puccetti, S., Rodriguez Castillo, G. A., Salvetti, D., Tiengo, A., Zampieri, L., D'Agostino, D., Greiner, J., Haberl, F., Novara, G., Salvaterra, R., Turolla, R., Watson, M., Wilms, J., & Wolter, A. 2016, *ArXiv e-prints*
- Israel, G. L., Papitto, A., Esposito, P., Stella, L., Zampieri, L., Belfiore, A., Rodríguez Castillo, G. A., De Luca, A., Tiengo, A., Haberl, F., Greiner, J., Salvaterra, R., Sandrelli, S., & Lisini, G. 2017, *MNRAS*, 466, L48
- Jiang, Y.-F., Stone, J. M., & Davis, S. W. 2013, *ApJ*, 767, 148
- . 2014, *ApJ*, 796, 106
- Kato, Y., Hayashi, M. R., & Matsumoto, R. 2004, *ApJ*, 600, 338
- Kawashima, T., Mineshige, S., Ohsuga, K., & Ogawa, T. 2016, *PASJ*, 68, 83
- King, A. & Lasota, J.-P. 2016, *MNRAS*, 458, L10
- Lesur, G. & Longaretti, P.-Y. 2007, *MNRAS*, 378, 1471
- Levermore, C. D. 1984, *JQSRT*, 31, 149
- Lyutikov, M. 2014, *ArXiv e-prints*
- McKinney, J. C., Tchekhovskoy, A., Sadowski, A., & Narayan, R. 2014, *MNRAS*, 441, 3177
- Narayan, R. & Yi, I. 1994, *ApJL*, 428, L13
- Ohsuga, K. 2007, *PASJ*, 59, 1033
- Ohsuga, K. & Mineshige, S. 2007, *ApJ*, 670, 1283
- Ohsuga, K. & Takahashi, H. R. 2016, *ApJ*, 818, 162
- Penna, R. F., McKinney, J. C., Narayan, R., Tchekhovskoy, A., Shafee, R., & McClintock, J. E. 2010, *MNRAS*, 408, 752
- Penna, R. F., Sądowski, A., Kulkarni, A. K., & Narayan, R. 2013, *MNRAS*, 428, 2255
- Romanova, M. M., Ustyugova, G. V., Koldoba, A. V., & Lovelace, R. V. E. 2009, *MNRAS*, 399, 1802
- . 2011, *MNRAS*, 416, 416
- . 2012, *MNRAS*, 421, 63
- Rykoff, E. S., Aharonian, F., Akerlof, C. W., Ashley, M. C. B., Barthelmy, S. D., Flewelling, H. A., Gehrels, N., Göğüş, E., Güver, T., Kiziloğlu, Ü., Krimm, H. A., McKay, T. A., Özel, M., Phillips, A., Quimby, R. M., Rowell, G., Rujopakarn, W., Schaefer, B. E., Smith, D. A., Vestrand, W. T., Wheeler, J. C., Wren, J., Yuan, F., & Yost, S. A. 2009, *ApJ*, 702, 489
- Sądowski, A. & Narayan, R. 2015, *MNRAS*, 454, 2372
- Sądowski, A., Narayan, R., McKinney, J. C., & Tchekhovskoy, A. 2014, *MNRAS*, 439, 503
- Sądowski, A., Narayan, R., Tchekhovskoy, A., Abarca, D., Zhu, Y., & McKinney, J. C. 2015, *MNRAS*, 447, 49
- Sądowski, A., Wielgus, M., Narayan, R., Abarca, D., McKinney, J. C., & Chael, A. 2017, *MNRAS*, 466, 705
- Shakura, N. I. & Sunyaev, R. A. 1976, *MNRAS*, 175, 613
- Shapiro, S. L. & Teukolsky, S. A. 1986, *Black Holes, White Dwarfs and Neutron Stars: The Physics of Compact Objects*, 672
- Simon, J. B. & Hawley, J. F. 2009, *ApJ*, 707, 833
- Takahashi, H. R. & Ohsuga, K. 2015, *PASJ*, 67, 60
- Takahashi, H. R., Ohsuga, K., Kawashima, T., & Sekiguchi, Y. 2016, *ApJ*, 826, 23
- Takahashi, H. R., Ohsuga, K. 2017, submitted to *ApJ*
- Thorne, K. S. 1981, *MNRAS*, 194, 439
- Wasserman, I. & Shapiro, S. L. 1983, *ApJ*, 265, 1036
- Watarai, K.-y. & Fukue, J. 1999, *PASJ*, 51, 725